Supplementary Materials for

Clonal hematopoiesis is associated with protection from Alzheimer's disease

Hind Bouzid[1], Julia A Belk[2], Max Jan[3], Yanyan Qi[1], Chloé Sarnowski[4], Sara Wirth[1], Lisa Ma[1], Matthew Chrostek[1], Herra Ahmad[1,5], Daniel Nachun[1], Winnie Yao[1], NHLBI Trans-omics for Precision Medicine (TOPMed) Consortium, Alexa Beiser[6], Alexander Bick[7], Joshua C. Bis[8], Myriam Fornage[9], William T. Longstreth, Jr.[10], Oscar L. Lopez[11], Pradeep Natarajan[12,13], Bruce M. Psaty[8], Claudia L. Satizabal[14], Joshua Weinstock[15], Eric B. Larson[16], Paul K. Crane[17], C. Dirk Keene[18], Sudha Seshadri[14], Ansuman T. Satpathy[1], Thomas J. Montine[1], Siddhartha Jaiswal[1,19]*

Correspondence to: sjaiswal@stanford.edu

This PDF file includes:

Materials and Methods
Figs. S1 to S6
Tables S1 to S14

Materials and Methods

Cohort descriptions

Framingham Heart Study

The FHS is a single-site, prospective and population-based study that has followed participants from the town of Framingham, MA to investigate risk factors for cardiovascular diseases. The population of Framingham was almost entirely white at the beginning of the study. The FHS comprises three generations of participants. The first generation (Original cohort/Gen1)(*25*), followed since 1948, enrolled 5,209 men and women who comprised two-thirds of the adult population then residing in Framingham, MA, USA. Survivors continue to receive biennial examinations. The second generation (Offspring cohort/Gen2)(*26*), followed since 1971, comprised 5,124 offspring of Gen1 and spouses of the offspring (including 3,514 biological offspring) who attended examinations every 4 to 8 years. The third generation (Gen3)(*27*) , enrolled in 2002, included 4,095 children from the largest offspring families who attended three examinations 4 years apart. All cohorts continue under active surveillance for cardiovascular events, stroke, and dementia. All participants provided written informed consent at each examination.

A total of 4,195 samples were sequenced as part of the Trans-omics for Precision Medicine (TOPMed) project Freeze 6 release as previously described (*7*). The selection of participants for sequencing was mostly a random selection of those with available DNA, but also included some related individuals for family studies. After exclusion of participants with coronary heart disease, ischemic stroke, or with missing information on age at blood draw or Alzheimer's disease (AD) diagnosis, a total of 2,437 persons remained for this analysis. Adjudication for Alzheimer's phenotypes was done by a committee (*28*), comprising at least two neurologists and a neuropsychologist. Multiple types of information were used to evaluate participants with suspected dementia, including neurologic and neuropsychological assessments, a telephone interview with a family member or care

giver, medical records, imaging studies, and autopsy data when available. AD was diagnosed when participants met the criteria of the National Institute of Neurological and Communicative Disorders and Stroke (**NINCDS**) and the Alzheimer's Disease and Related Disorders Association (**ADRDA**) for definite, probable, or possible Alzheimer's disease.

Data for FHS are available in dbGaP:

https://www.ncbi.nlm.nih.gov/projects/gap/cgi-bin/study.cgi?study_id=phs000974.v1.p1

Cardiovascular Health Study

The CHS is a prospective, multi-ethnic, longitudinal study of risk factors for coronary heart disease and stroke in people aged 65 and older. A total of 2,840 samples were sequenced as part of the Trans-omics for Precision Medicine (TOPMed) project as previously described (*7*).The samples selected for whole genome sequencing as part of TOPMed were heavily oversampled for cardiovascular disease cases. After exclusion of participants with coronary heart disease or stroke, or with missing information on age at blood draw or AD diagnosis, a total of 743 persons remained for this analysis. Alzheimer's disease was diagnosed as probable and possible following the NINCDS-ADRDA criteria in 1997-98 and 2002-03 (*29*).

Data for CHS are available in dbGaP:

https://www.ncbi.nlm.nih.gov/projects/gap/cgi-bin/study.cgi?study_id=phs001368.v2.p2

Written informed consent was obtained from all human participants by each of the studies that contributed to TOPMed. Each study received institutional certification before deposition in dbGaP, which certified that all relevant institutional ethics committees approved the individual studies and that the genomic and phenotypic data submission was compliant with all relevant ethical regulations. Secondary analysis of the dbGaP data in this manuscript was approved by the Stanford University Institutional Review Board, and this work is compliant with all relevant ethical regulations.

ADSP

The Alzheimer's Disease Sequencing Project (ADSP) is a collaborative effort of the National Institutes of Aging, the National Human Genome Research Institute, and the Alzheimer's community to understand the genetic basis of AD (*13*). The whole exome sequencing (WES) set of ADSP was a case-control design where cases met NINCDS-ADRDA criteria for possible, probable, or definite AD, had documented age at onset or age at death, and *APOE* genotyping. A case-control selection strategy was chosen that targeted cases with minimal risk as predicted by known risk factors (age, sex, and *APOE*) and targeted controls with the least probability of conversion to AD by age 85 years (*13*). A total of 5,096 cases and 4,965 controls from 24 cohorts were chosen for WES. As a result of this selection strategy, cases and controls were not well-matched for age, except for carriers of *APOE* ε3ε3 genotype. Furthermore, 1,776 samples were sequenced from brain, not blood, DNA. We limited our CHIP/AD association analysis to those samples where DNA was derived from blood and where age at blood draw used for sequencing was known. In most cases, the AD diagnosis was made prior to the blood draw, however the diagnosis was usually within 5 years of the time of blood sampling for both prevalent and incident cases. After excluding those without blood DNA or known age at blood draw and further limiting to *APOE* ε3ε3 carriers, we had 1,104 AD cases and 1,446 controls who were well matched by age.

Written informed consent was obtained from all human participants by each of the studies that contributed to ADSP. Secondary analysis of the dbGaP data in this manuscript was approved by the Partners Healthcare Institutional Review Board, and this work is compliant with all relevant ethical regulations.

Data for ADSP is available in dbGaP:

https://www.ncbi.nlm.nih.gov/projects/gap/cgi-bin/study.cgi?study_id=phs000572.v8.p4

Variant calling and annotation

Whole genome sequencing for TOPMed samples was performed as previously described (*12*). FASTQ files were aligned to hg38 for TOPMed WGS and hg19 for ADSP and the resulting BAM files were passed through Mutect/Indelocator (ADSP) or Mutect2 (TOPMed) pipelines to identify putative variants as previously described (*6*). Briefly, the Mutect/Mutect2 pipelines excluded variants that had characteristics of common artifacts, such as oxoguanine artifact, end of read artifact, and PCR artifact (strand bias). Common polymorphisms present in germline databases were also excluded. Rare error modes were excluded by using a Panel of Normals compiled from persons without CHIP in the same sequencing centers. Output from the Mutect/Mutect2 pipelines were then annotated for known CHIP variants in 73 genes from a curated whitelist (Supplemental Table 1).

Statistical analysis plan

TOPMed

We wished to test for an association of AD dementia to CHIP. We hypothesized that CHIP carriers would have increased risk of AD dementia based on prior data that CHIP carriers have more inflammation in innate immune cells (*6*, *7*, *9*) and that enhanced inflammasome activation was associated with worsened AD phenotypes in mice (*30*).

For the discovery set, we utilized the two cohorts in TOPMed, FHS and CHS. The CHS sample was heavily oversampled for those with cardiovascular diseases, especially coronary heart disease (CHD) and stroke (1,838 out of 2,840 participants had these conditions). CHIP is known to be associated with atherosclerotic cardiovascular disease (*6*). As systemic atherosclerosis is a risk factor for vascular dementia, which can mimic AD dementia symptoms, we wished to exclude anyone with these conditions to prevent confounding. To do this, we excluded anyone with an event type of myocardial infarction (MI), stroke, angioplasty, coronary artery bypass surgery, silent MI, or death due to coronary heart disease using CHS event codes (https://www.ncbi.nlm.nih.gov/projects/gap/cgi-bin/variable.cgi?study_id=phs000287.v2.p1&phv=100824&phd=2793&pha=3548&pht=1466&phvf=&phdf=&phaf=&phtf=&dssp=1&consent=&temp=1) and excluded those selected on the basis of CHD, stroke, or "other"

sampling group codes (https://www.ncbi.nlm.nih.gov/projects/gap/cgi-bin/variable.cgi?study_id=phs001368.v2.p2&phv=377683&phd=8024&pha=&pht=7957&phvf=&phdf=&phaf=&phtf=&dssp=1&consent=&temp=1). For FHS, we also excluded anyone with codes for coronary heart disease or ischemic stroke.

FHS and CHS are both prospective studies with information on incident AD diagnosis. We therefore utilized regression models to test for an association of CHIP to incident AD dementia in both cohorts. After excluding those without information on AD diagnosis, there were 2,437 persons in FHS and 620 persons in CHS. Other variables included in these models were age at blood draw used for sequencing, *APOE* genotype, and sex. The results from both cohorts were then meta-analyzed using a fixed-effects meta-analysis. To exclude confounding due to survivorship bias, we performed the analysis using competing risks regression, with death as the competing risk. The R packages survival (https://cran.r-project.org/web/packages/survival/index.html), meta (https://cran.r-project.org/web/packages/meta/index.html), and cmprsk (https://cran.r-project.org/web/packages/cmprsk/index.html) were used to perform the Cox models, meta-analysis, and competing risks regression (CRR), respectively. Visual examination of a plot of the Schoenfeld residuals revealed that the proportional hazards assumption was met for each covariate. For FHS, some participants were selected as part of family studies, which could potentially lead to biased estimates in the regression models due to correlated genetic or environmental factors. To control for this possibility, we also included family as a cluster variable in the CRR model for FHS using the R package crrSC (https://cran.r-project.org/web/packages/crrSC/index.html) and obtained very similar results as with the un-clustered model (Table S4). Therefore, we omitted family as a variable for additional analyses.

ADSP

Having demonstrated a surprising inverse association between CHIP and AD dementia in the discovery set, we wished to replicate the finding. For this, we utilized the ADSP data. As described above, carriers of *APOE* ε2 or *APOE* ε4 alleles were selected in such a way that cases and controls were poorly matched for age. Due to this selection bias, carriers of these alleles were excluded from the analysis. However, *APOE* ε3ε3 carriers were well matched for age, allowing for us to use this set as the replication cohort. We further excluded those without blood as the source for DNA and those without a known age at blood draw used for sequencing. A major difference between ADSP and TOPMed is the use of higher depth whole exome sequencing in ADSP, compared to lower depth whole genome sequencing in TOPMed. In order to perform a power calculation for the replication study in ADSP, we had to ensure the variant allele fraction was comparable between ADSP and TOPMed for two reasons. First, the sensitivity to detect CHIP is linked to the sequencing depth, therefore the prevalence of CHIP was higher in ADSP. Second, the associations for previously studied health outcomes related to CHIP are dependent on clone size, with small clones having less of an effect size. We empirically determined that a cutoff of VAF at 0.08 gave a nearly identical VAF distribution for CHIP clones in ADSP as compared to TOPMed.

After these exclusions, we had 2,550 persons in ADSP for the analysis, of whom 43% were AD cases and 17% were CHIP carriers at a VAF>0.08. We then used the powerMediation (https://cran.r-project.org/web/packages/powerMediation/index.html) package in R to perform a power calculation for varying effect sizes of CHIP at an alpha of 0.1. For an odds ratio of 0.6 (similar to the hazard ratio for CHIP obtained from TOPMed), the power was 1. For an odds ratio of 0.8, the power was 0.96. For an odds ratio of 0.9, the power was 0.50. Thus, we were well-powered for the replication analysis in ADSP. We used logistic regression to assess for the association between CHIP and AD in ADSP, with age at blood draw and sex as other explanatory variables in the model. For privacy concerns, those age 90 or older did not have an exact age available on dbGaP, and were considered to be age 90 for the purposes of this analysis.

We further assessed whether smaller clones were associated with AD dementia in two ways. First, we performed a logistic regression for AD where CHIP status was modeled as a three-factor variable (no CHIP, CHIP with VAF≤0.08, or CHIP with VAF>0.08). Second, we performed a logistic regression for AD dementia where VAF was included as a continuous variable.

A fixed-effects meta-analysis for risk of AD in CHS, FHS, and ADSP was performed using logistic regression models for each cohort with age at blood draw, sex, APOE genotype and CHIP carrier status as covariates.

We wished to test whether CHIP status was associated with AD-related pathologic changes in people without clinical dementia symptoms. For a subset of participants in ADSP who died and donated their brains for research, a neuritic plaque score based on the Consortium to Establish a Registry for Alzheimer's Disease (CERAD) criteria and Braak stage was assessed. For this analysis, we utilized all *APOE* genotypes and limited the analysis to those with available age at autopsy. Information on CERAD score was obtained from the National Alzheimer's Coordinating Center Alzheimer's Disease Research Centers (NACC/ADRC) and the Adult Changes in Thought (ACT) cohort. Information on Braak stage was available from NACC/ADRC, ACT, FHS, and the Genetic Differences cohort. For all cohorts, anyone with a clinical dementia diagnosis was excluded. For NACC/ADRC and ACT, we also excluded anyone with mild cognitive impairment. A total of 427 cases had CERAD neuritic plaque scores and 454 cases had Braak stages available for this analysis after these exclusions. We performed ordinal logistic regression for CERAD score (0-3) and Braak stage (grouped as 0/I/II, III/IV, V/VI) using the polr function in the MASS package in R (https://cran.r-project.org/web/packages/MASS/index.html). Explanatory variables included CHIP, age at death, sex, and *APOE* genotype. The t-values from the ordinal logistic model were used to calculate p-values for each of the covariates using a standard normal distribution.

Mendelian randomization

Data from Bick et al. (*7*)was used to select variants for the CHIP instrumental variable and data from Schwartzentruber et al. (*16*) provided summary statistics from a large AD GWAS/GWAX meta-analysis. The AD GWAS included ~22,000 AD cases and ~42,000 controls from Kunkle et al.(*31*), while the GWAX contained ~53,000 AD-by-proxy cases and ~378,000 controls from UK Biobank. We defined variants as being independent if they had a linkage disequilibrium (LD) R^2 value of less than 0.2 in TOPMed (http://topld.genetics.unc.edu/topld/). We selected the lead variant at each independent locus, or a variant in high LD (R^2>0.9) with the lead variant if the lead variant was not represented in the array data from all cohorts used in the AD GWAS/GWAX. We also excluded variants from the CHIP GWAS that were primarily restricted to African ancestry, since the AD GWAS summary statistics were obtained from Europeans. We identified three loci that met these criteria, two at the *TERT* locus (rs2853677 and rs7726159) and one at the *KPNA4*/*TRIM59* locus (rs58322641). The beta values and standard errors for these three variants from the CHIP and AD GWAS summary statistics were then used to perform inverse-variance weighted Mendelian randomization using the MendelianRandomization package (https://cran.r-project.org/web/packages/MendelianRandomization/index.html).

Nuclei isolation from human postmortem brain tissue

ACT is a longitudinal, community-based observational study of brain aging in participants older than 65 randomly sampled from the Group Health Cooperative (now Kaiser Permanente), a health management organization in King County, Washington. A subset of participants in the study donate their brains for research upon death, and a comprehensive neuropathological exam is performed to assess for AD and related neurodegenerative disease pathologies (*32*). For decedents with post-mortem interval of less than 8 hours, a rapid autopsy is performed in which numerous samples from multiple brain regions are taken from one hemisphere and flash frozen in liquid nitrogen.

For this analysis, we obtained occipital cortex samples from 9 ACT brain donors (8 CHIP carriers and 1 non-carrier). Three of these also had a frozen sample from cerebellum available, and 2 had a frozen sample from the

putamen. For nuclei isolation, we performed and adapted the protocol from (*33*). Briefly, around 250 mg of frozen postmortem brain tissue was thawed in 5 mL lysis buffer and transferred to a douncer placed on ice. After 20-30 strokes, the homogenized tissue was transferred to a clear 50 mL ultracentrifuge tube and the volume was adjusted to 12 mL. 21 mL of sucrose buffer was added to the bottom of the clear ultracentrifuge tube, to create a concentration gradient with the homogenized tissue solution on top of the sucrose buffer. The tubes were placed in buckets in a SW32Ti swinging rotor (Beckton Dickinson). The samples were ultracentrifuged at 107163.6 RCF for 2.5 hours at 4°C. The supernatant was removed and 500 µL of 1X PBS was added to the pellet and incubated for 20 min on ice. The nuclei were then resuspended and transferred into a microcentrifuge tube. The nuclei were counted using trypan blue dilution and then centrifuged at 500G for 5 min.

Lysis buffer: 0.32M Sucrose, 5 mM CaCl2, 3 mM Mg(Acetate)$_2$, 0.1 mM EDTA, 10mM Tris-HCl pH8, 1 mM DTT, 0.1%Triton X-100 in H20.

Sucrose buffer: 1.8 M Sucrose, 3 mM Mg(Acetate)$_2$, 1 mM DTT, 10 mM Tris-HCl, pH8 in H20

Immunostaining and sorting of the nuclei

The nuclei were resuspended at a concentration of 200,000 cells in 50ul of 0.5% BSA in 1x PBS solution and stained for 45 min with Anti-NeuN Antibody Alexa Fluor 488(EMD Millipore) at a concentration of 1: 400, and Anti-C-MAF antibody PE (BD biosciences) at a concentration of 1: 50. The nuclei were then washed and strained using a 40um strainer. The sorting was done on an Aria II sorter using a 100um nozzle. The nuclei were collected in 0.5% BSA in 1x PBS solution and centrifuged at 500G for 5 min.

DNA extraction, amplification and sequencing

DNA was extracted from the nuclei using the Qiagen QIAmp DNA micro kit. DNA concentration was measured using the Qubit fluorometer. PCR was performed to amplify the region surrounding the mutation of interest (around 300bp) using the Phusion high fidelity master mix (New England Biolabs). The amplified DNA was purified using the Qiagen QIAquick PCR purification kit according to the manufacturer recommendations.

Libraries were generated from the pooled amplicons using the Celero DNA-seq library kit (NuGEN). Sequencing of the libraries was performed using MiSeq Nano v2 kits. Sequencing reads were aligned with BWA (http://bio-bwa.sourceforge.net), and variant calling and annotation done with Varscan (http://varscan.sourceforge.net) and Annovar (https://annovar.openbioinformatics.org/en/latest/).

DNMT3A p.L859* : 5'- CCAGTGTTGGCTGGTGAATG-3', 5'-TAAAACCCACTGTTCCCAGGAC-3'

DNMT3A p.R635P : 5'-CAGGGTGTGTGGGTCTAGGA-3', 5'-CACACACAAGCTTCCCCTTT-3'

DNMT3A p.Y735: 5'-GGGACAGCTATTCCCGATGA-3', 5'-TAGAAGCCATTAGTGAGCTGGC-3'

SF3B1 p.H662Q : 5'-TGTCCGTAACACAACAGCTAGA-3', 5'-AGCCCAAAGGTTTGAGTCC-3'

TET2 p.C1193Y : 5'-TTGCCTCTTGAATTCATTTGCT-3', 5'-TGCCTCTTCTTAAGAGATAACACA-3'

TET2 p.KL1818fs : 5'-GGCATGTTCAACAGCTCTCT-3', 5'-ATTGACCCATGAGTTGGAGCC-3'

ASXL1 p.S444* : 5'-ACAGCGAGATGGGCATTTTA-3', 5'-CACGTGCCAAGTTGTCTGG-3'

TET2 p.A1355V : 5'-GTGTCATTCCATTTTGTTTCTGGA-3', 5'-GCTGTCCTCAGCCCAACTTA-3'

DNMT3A p.T538fs : 5'-GGAGGCCAAGGTGTGCTAC-3', 5'- GGGTCATGTCTTCAGGGCTTAG-3'

GNB1 p.K57E : 5'- AGAGCAGCCCCTGAATGTAAC-3', 5'-GTTCAGTGCAGAATGCCACA-3'

scATAC-seq

Sample processing

After nuclei isolation as described above, samples were transposed, single cells were barcoded using 10X Genomics GEMs (Gel Bead in-EMulsions), and libraries were prepared for sequencing according to the commercially available 10X Chromium™ Next GEM Single Cell ATAC Library & Gel Bead Kit v1.1. Paired end sequencing was performed on an Illumina HiSeq 2500.

Analysis pipeline

Fastq files were trimmed, deduplicated, filtered and aligned using the 10X cellranger-atac count pipeline, yielding a file of high quality ATAC-seq fragments for all cells per sample. Reference genome hg19 was used for

compatibility with the hematopoiesis reference dataset (described below(*23*)). The fragments file for each sample was then loaded into ArchR for downstream analysis (*34*).

Cell quality control and clustering was performed using the standard ArchR pipeline. Briefly, barcodes were called as cells based on fragments per barcode and enrichment of fragments in transcription start sites (TSS) genome wide. For each sample, doublets were predicted and removed based on similarity to computationally simulated doublets. The TileMatrix and GeneScoreMatrix were computed using default settings. For the GeneScoreMatrix, imputation was performed using the ArchR implementation of MAGIC to aid visualization of the sparse ATAC-seq signals in single cells. Dimensionality reduction and clustering was performed using the TileMatrix, which tiles the genome into 500 bp windows. Although Harmony batch correction is implemented and part of the standard workflow in ArchR, we did not use any batch correction to ensure that any biological differences between the samples would be preserved. After clustering, reproducible peaks were determined for each cluster individually to ensure that cell type specific peaks were retained. Reproducible peaks for each cluster were merged into a set of disjoint, fixed width (500bp) peaks which were used to create the cell by peak matrix. ATAC-seq pseudo-bulk tracks for selected groups of cells were exported from ArchR using the `getGroupBW` function. All tracks were identically normalized using ReadsInTSS, which corrects for variation in sequencing depth and also cell quality between different groups of cells. Specific regions in the genome were visualized using the Integrative Genomics Viewer (https://software.broadinstitute.org/software/igv/).

To quantify differences between samples within cluster 9 (the analysis shown in Fig. S6C), we used `ArchR::getMarkerFeatures` for every pair of samples in this study, and also every pair of samples in the Corces 2020 data. To control for the different cell numbers within cluster 9 for the different samples, the number of cells considered (per sample) was capped using `maxCells=114`, with 114 being the lowest number of cells present across any sample (ACT6 P, Table S13). We then counted the number of peaks passing thresholds FDR < 0.1, abs(log2(fold change)) > 1 for each pairwise comparison.

Reference datasets

To aid in interpretation of cell types from our scATAC-seq data, we incorporated two previously published datasets (*21*),(*23*). For the Corces et. al. brain dataset, original fastq files of all 10 scATAC samples (available under GEO accession no. GSE147672) were aligned to the hg19 reference genome and then processed as described above. For the Satpathy et. al. hematopoiesis dataset, we downloaded fragments files for the 7 samples most relevant to our study, focusing on dendritic cells and monocytes. Accession numbers and sample names of these are:

GSM3722015_PBMC_Rep1_fragments.tsv.gz

GSM3722076_PBMC_Rep2_fragments.tsv.gz

GSM3722075_PBMC_Rep3_fragments.tsv.gz

GSM3722077_PBMC_Rep4_fragments.tsv.gz

GSM3722039_Dendritic_all_cells_fragments.tsv.gz

GSM3722026_Dendritic_Cells_fragments-Reformat.tsv.gz

GSM3722027_Monocytes_fragments.tsv.gz

These fragments files were processed in ArchR as described above. After clustering, we identified the predominant dendritic cell cluster and the predominant monocyte cluster based on expression of marker genes and the known sorted sample types. For example, the monocyte cluster contained nearly all cells from the monocyte sample (GSM3722027) as well as cells from the PBMC samples. Normalized bigwig files for each cluster were exported and visualized as described above.

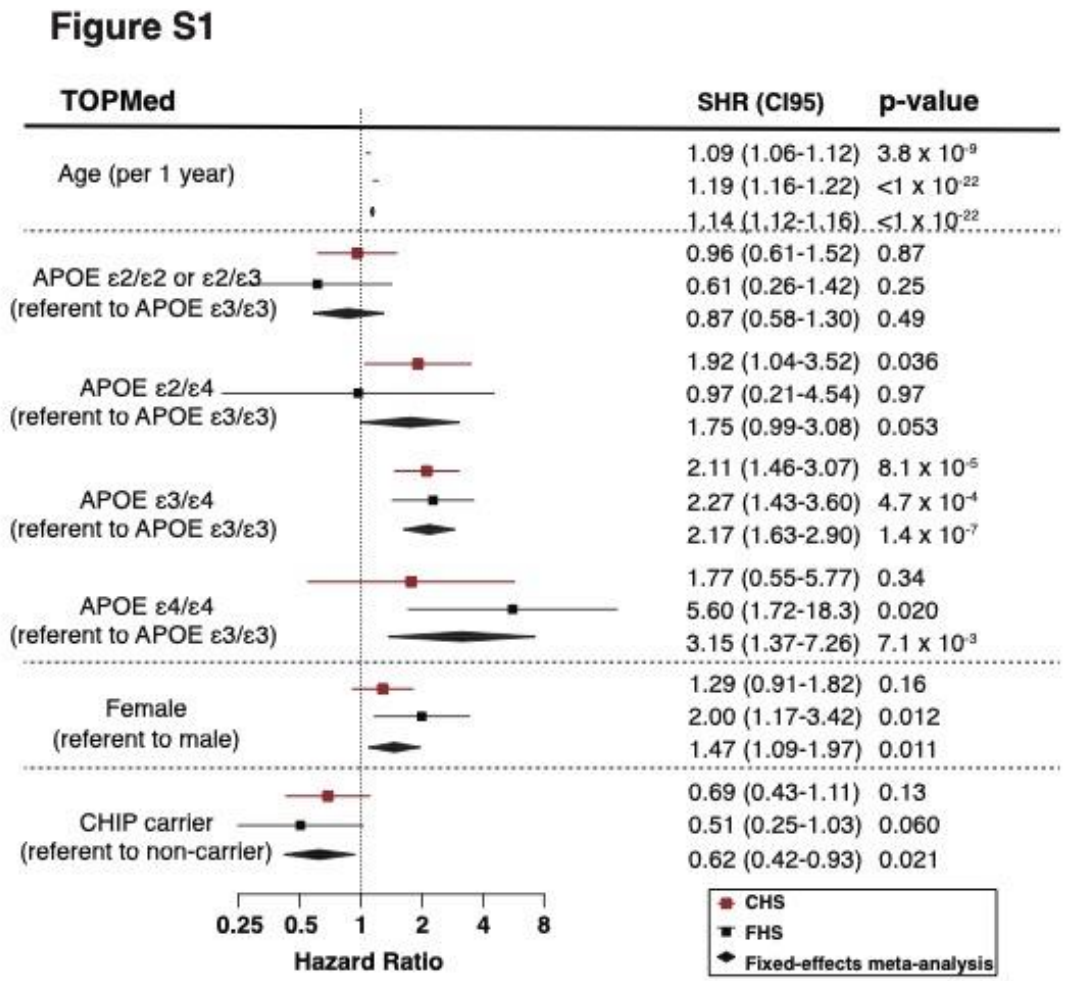

Fig. S1. CHIP is associated with protection from AD in CHS and FHS
Forest plot of risk factors for incident Alzheimer's disease (AD) in Cardiovascular Health Study (CHS) and Framingham Heart Study (FHS). The covariates included in the model (age at time of whole genome sequencing blood draw, *APOE* genotype, sex, and CHIP status) are shown. Hazard ratios (HR), 95% confidence intervals (CI95) and Wald p-values were calculated for each covariate from Cox proportional hazards regression models, which were then meta-analyzed using a fixed-effects model for the two cohorts.

Figure S2

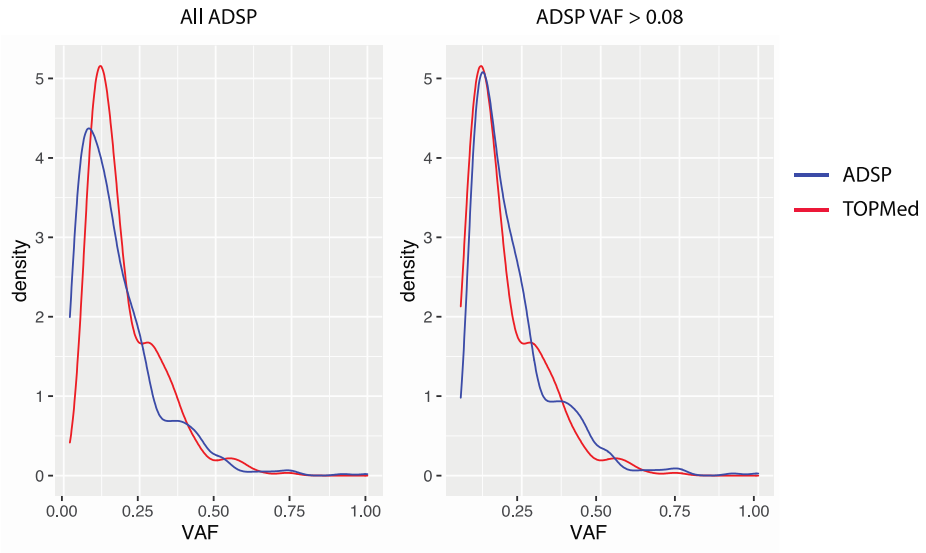

Fig. S2. The VAF distribution is different in TOPMed and ADSP due to higher sequencing depth in ADSP Density plots of VAF from all CHIP carriers in ADSP (left) or in CHIP carriers with VAF greater than 0.08 (right) compared to VAF distribution from TOPMed CHIP carriers (red) in each plot.

Figure S3

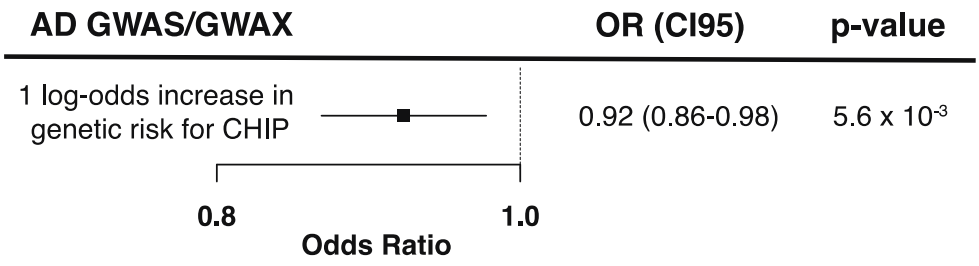

Fig.S3. Mendelian randomization demonstrates that genetic risk of CHIP is associated with protection for AD

Three independent genome-wide significant variants for CHIP were used to perform inverse-variance weighted Mendelian randomization on summary statistics from Schwartentruber et al. Results are presented as odds ratio (OR) for risk of AD per 1 log-odds increase in genetic risk of CHIP, with 95% confidence interval (CI95).

Figure S4

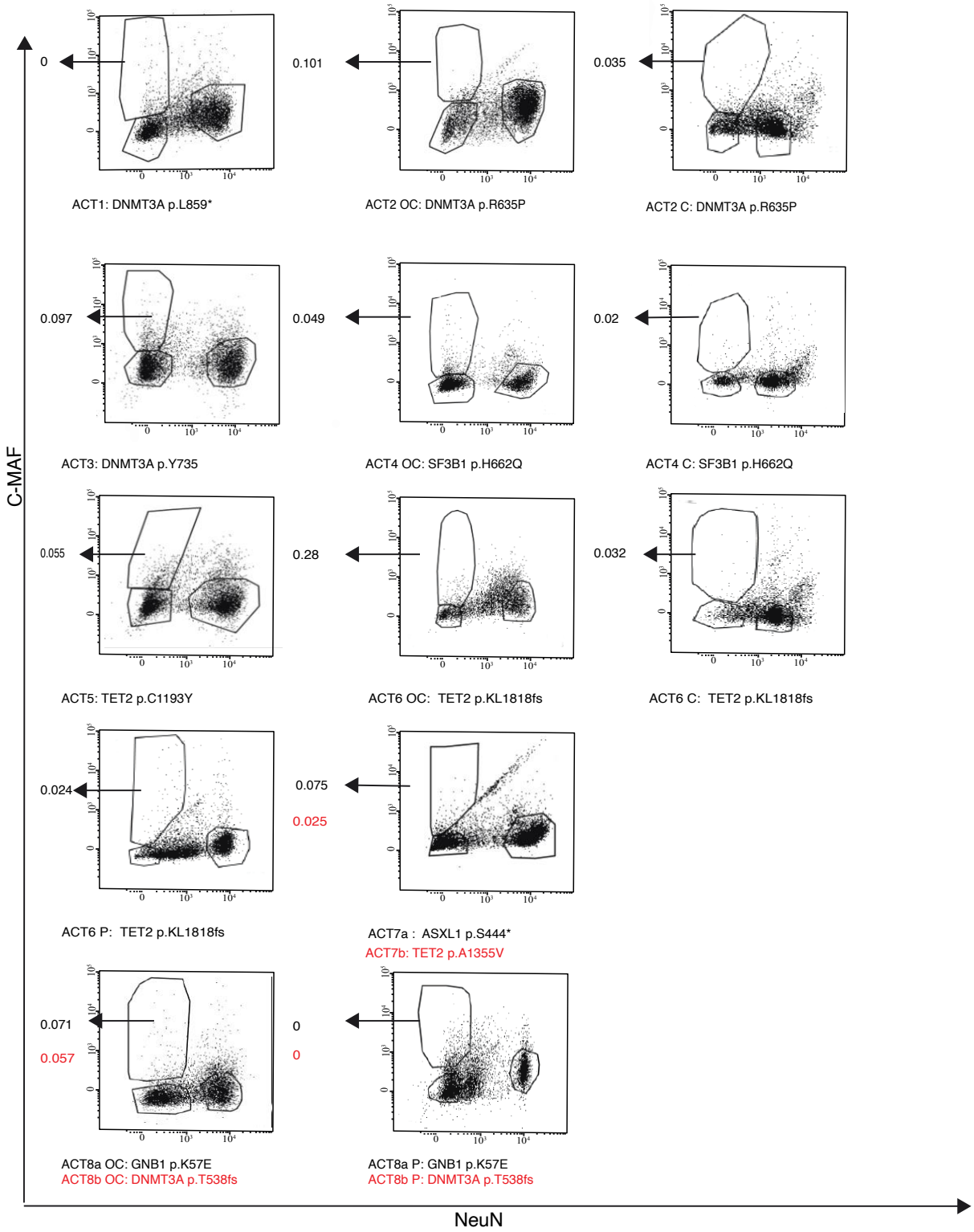

Fig. S4. Sorting of nuclei from brains of CHIP carriers can be used to enrich for the mutant cells
Flow cytometry gating strategy for nuclei sorting for the 8 brain samples using C-MAF and NeuN markers. The arrow points to the C-MAF^{+} NeuN^{-} sorted population and the VAF is indicated for each sample. The brain regions are abbreviated as Ce for Cerebellum, OC for Occipital cortex, and P for putamen.

Figure S5

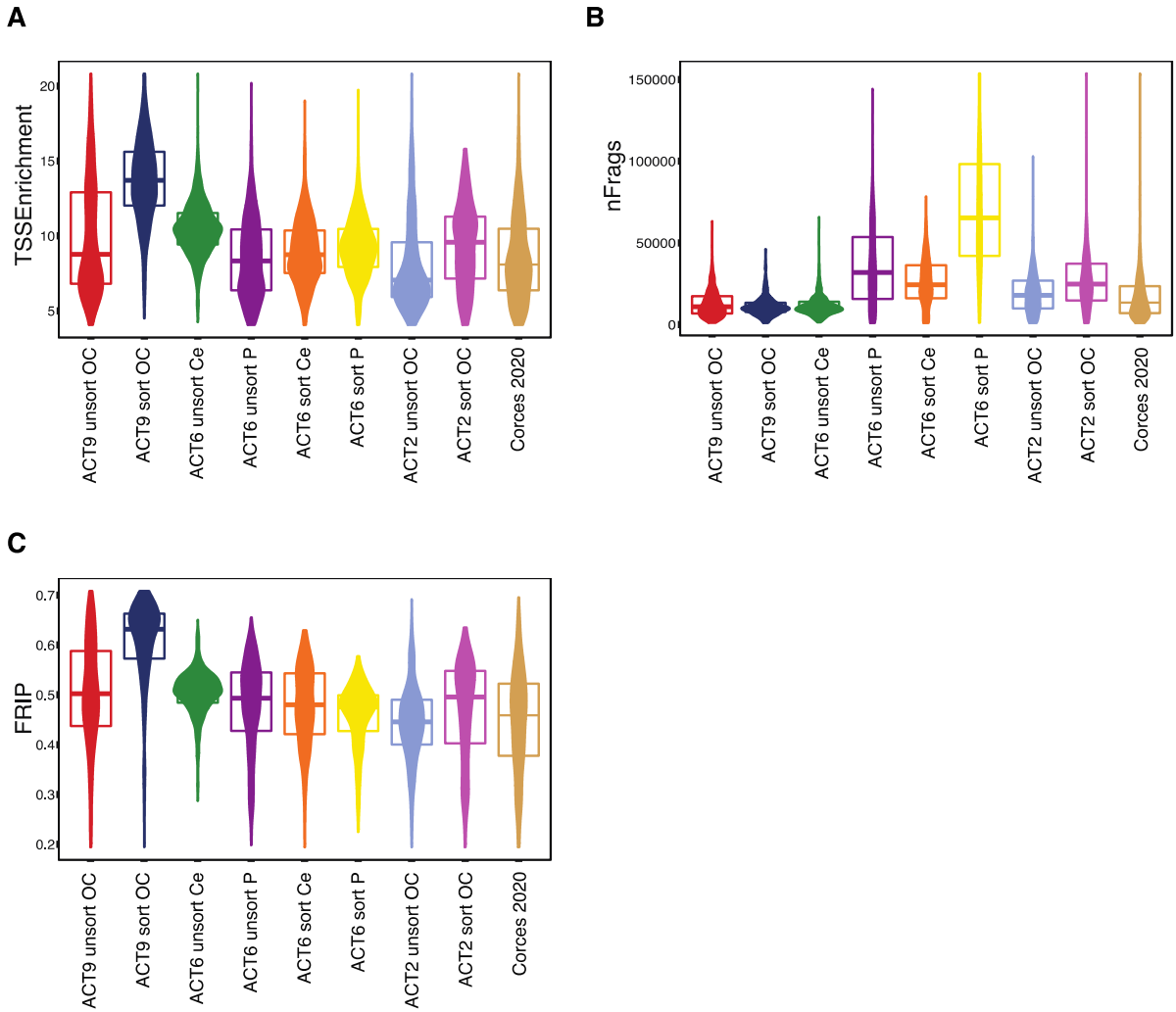

Fig. S5. High-quality scATAC-seq libraries from ACT brain samples
Quality control metrics for each cell in the indicated scATAC-seq sample. Aggregated Corces 2020 samples are included for reference. (A) Enrichment of fragments in transcription start sites (TSS), (B) number of fragments, and (C) fraction of reads in peaks (FRIP) for each cell.
The brain regions are abbreviated as Ce for Cerebellum, OC for Occipital cortex, and P for putamen.

Figure S6

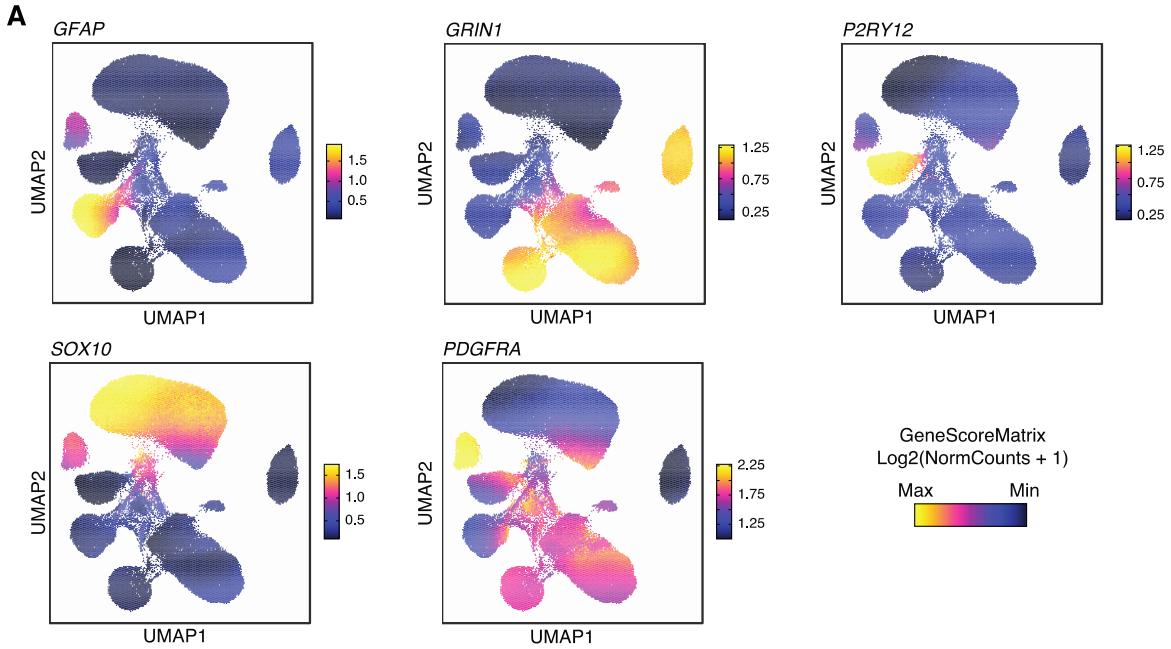
A
GFAP
GRIN1
P2RY12
SOX10
PDGFRA
UMAP1
UMAP2
1.5
1.0
0.5
1.25
0.75
0.25
2.25
1.75
1.25
GeneScoreMatrix
Log2(NormCounts + 1)
Max
Min

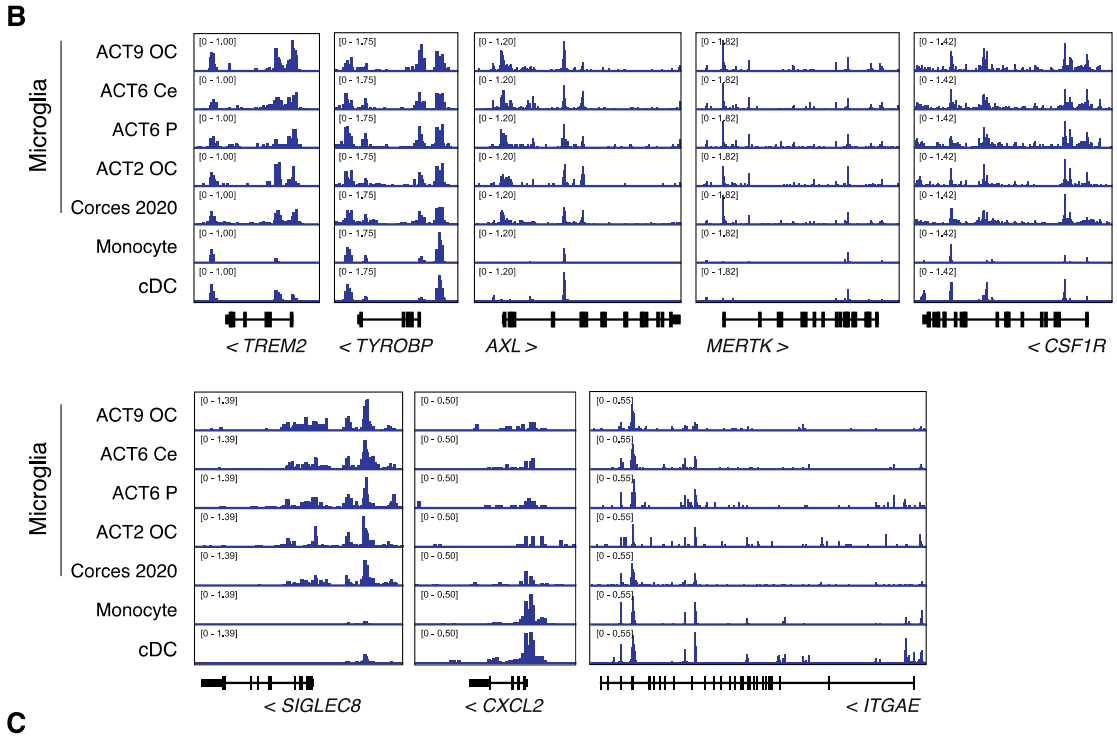
B
Microglia
ACT9 OC
ACT6 Ce
ACT6 P
ACT2 OC
Corces 2020
Monocyte
cDC
< TREM2
< TYROBP
AXL >
MERTK >
< CSF1R
< SIGLEC8
< CXCL2
< ITGAE

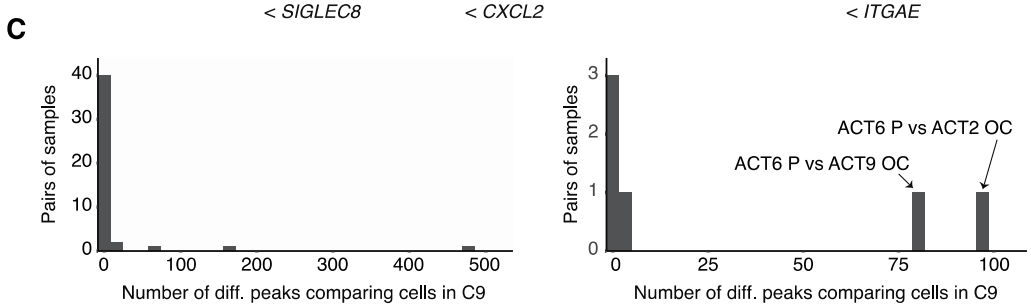
C
Pairs of samples
Number of diff. peaks comparing cells in C9
ACT6 P vs ACT2 OC
ACT6 P vs ACT9 OC

Fig. S6. Marker genes for scATAC-seq clusters

A) GeneScore markers used to identify cell types from scATAC-seq data.
B) Pseudo-bulk tracks shown for additional genes.
C) Histogram of the number of differential peaks (Wilcoxon test, FDR < 0.1, |log2(fold change)| > 1) comparing cells within Cluster 9 for different pairs of samples. Left: all pairs of Corces 2020 samples. Right: all pairs of samples generated in this study.

The brain regions are abbreviated as Ce for Cerebellum, OC for Occipital cortex, and P for putamen.

Table S1. List of hematopoietic genes and variants queried

Gene name	Reported mutations used for variant calling
ASXL1	Frameshift/nonsense/splice-site p.358-1541
ASXL2	Frameshift/nonsense/splice-site in p.380-1435
BCOR	Frameshift/nonsense/splice-site
BCORL1	Frameshift/nonsense/splice-site
BRAF	G464E, G464V, G466E, G466V, G469R, G469E, G469A, G469V, V471F, V472S, L485W, N581S, I582M, I592M, I592V, D594N, D594G, D594V, D594E, F595L, F595S, G596R, L597V, L597S, L597Q, L597R, A598V, T599I, V600M, V600L, V600K, V600R, V600E, V600A, V600G, V600D, K601E, K601N, R603*, W604R, W604G, S605G, S605F, S605N, G606E, G606A, G606V, H608R, H608L, G615R, S616P, S616F, L618S, L618W
BRCC3	Frameshift/nonsense/splice-site
CBL	RING finger missense p.381-421
CBLB	RING finger missense p.372-412
CEBPA	Frameshift/nonsense/splice-site
CREBBP	Frameshift/nonsense/splice-site, D1435E, R1446L, R1446H, R1446C, Y1450C, P1476R, Y1482H, H1487Y, W1502C, Y1503D, Y1503H, Y1503F, S1680del
CTCF	Frameshift/nonsense, R377C, R377H, P378A, P378L
CUX1	Frameshift/nonsense
DNMT3A	Frameshift/nonsense/splice-site, F290I, F290C, F290S, G293R, L295P, L295Q, L295V, V296G, V296L, V296M, W297C, W297L, W297R, W297G, G298W, G298R, G298E, W306C, P307S, P307R, P307L, P307T, G308D, I310F, I310L, I310S, I310T, S312F, R326G, R326H, R326L, R326C, R326S, V328A, V328D, V328G, F331V, G332R, G332E, S337A, S337L, S337P, V339A, V339M, V339G, L344Q, L344P, L344R, L347P, L347R, L347Q,S352N,Y365C, R366C, R366P, R366H, R366G, A368D, A368T, A368V, I369N, I369S, V372D, L373Q, A376P, A376T, A376V, R379H, R379L, R379C, R379S, D389N, I407T, I407N, I407S, W409R, A410D, A410T, G413V, F414L, F414I, F414S, F414V, F414C, K468R, E477Q, E477K, V483G, R484Q, R484W, C494Y, C497G, C497R, C497Y, G498E, H506R, G511E, C514Y, Q527H, Q527P, D529N, D529V, D531N, D531Y, Y533C, S535F, S535P, C537G, C537R, C540Y, G543A, G543S, G543C, G543D, G543V, L547H, L547P, L547F, L547R, C537Y, M548I, M548L, M548K, M548R, M548T, G542V,G550R, C554Y, R556K, R556S, R556G, C559R, C559Y, C562Y, V563M, P580L, W581R, W581G, W581C, W581S, C583S, C583Y, C586G, C586R, C586Y, K589N, L595P, R596W, R598Q, R604Q, R604W, P633H, P633L, I634F, I634T, R635G, R635L, R635P, R635W, R635Q, V636A, V636G, V636M, V636L, L637R, L637P, L637Q, S638F, S638P, S638Y, L639R, L639V, L639F, A644T, T645A, G646V, G646E, L647H, L648P, V649G, V649L, V649M, L650V, L650Q, L653W, L653F, I655N, I655T, Q656K, V657A, V657M, V657G, D658V, D658Y, R659C, R659G, R659H, Y660C, Y660N, Y660F, Y660H, Y660D, A662D, S663L, S663W, E664K, V665G, V665L, S669F, S669P, M674V, V675A, V675M, R676L, R676W, R676Q, I681N, I681S, I681M, M682R, Y683D, V684F, G685R, G685E, G685A, D686Y, D686G, D686H, D686V, V687L, D686A, V687F, R688C, R688G, R688H, V690G, V690F, V690D, T691I, I695N, H694Y, H694P, I695F I695T, Q696P,W698C, W698R, W698S G699R, G699S, G699D, G699V, P700L, P700S, P700R, P700Q, P700T, P700A, F701V, D702A, D702G. D702E, D702V, D702N, D702Y, L703P, L703R, L703V, V704A, V704M, V704G, I705F, I705T, I705S, I705N, G706E, G706W, G706R, G706V, G707C, G707D, G707S, G707R, G707V, C710S, C710Y, D712A, L713F, S714C, V716D, V716F, V716I, N717S, N717I, P718L, R720C, R720H, R720G, R720S, K721R, K721T, K721N, Y724C, E725K, G726V, G728D, R729Q, R729W, R729G, R729L, F731C, F731L, F731Y, F731I, F731V, F732del, F732C, F732I, F732S, F732L, F732V, E733G, E733A, E733V, F734L, F734C, F734V, Y735C, Y735N, Y735S, Y735F, Y735H, R736G, R736H, R736C, R736L, R736P, R736S, L737H, L737P, L737V, L737F, L737R, L737P, L738P, L738Q, H739P, A741G, A741V, R742L, R742G, R742P, P743H, P743R, P743L, P743S, R749C, R749L, R749H, R749G, P750R, F751L, F751C, F751I, F751V, F752del, F752C, F752L, F752I, F752V, W753G, W753C, W753L, W753R, W753S, L754P, L754R, L754H, F755S, F755I, F755L, M761I, M761V, G762C, V763G, V763I, K766E, D768E, D768H, D768V, D768Y, I769N, I769S, I769T, I769V, S770L, S770W, S770P, R771G, R771L, R771P, R771Q, F772C, F772I, F772V, L773H, L773I, L773R, L773V, E774A, E774K, E774D, E774G, E774V, S775F, S775P, P777A, P777H, P777L, P777R, P777T, P777S, V778M, I780N, I780S, I780T, D781G, V785M, A787G, A787S, H789Q, R790W, A791V, R792C, R792H, R792S, F794L, F794V, W795S, W795G, W795C, W795L, W795R, G796A, G796C, G796D, G796V, N797D, N797Y, N797H, L798P, L798H, N797K, N797S, P799L, P799A, P799T, P799S, P799R, P799H, G800S, M801I, M801R, M801T, M801V, R803S, R803G, R803K, R803T, R803W, R803M, P804L, P804S, L815Q, H821D, H821P, H821R, K826N, K826T, K826R, S828N, K829R
EED	Frameshift/nonsense, L240Q, I363M
EP300	Frameshift/nonsense, VF1148_1149del, D1399N, D1399Y, P1452L, Y1467N, Y1467H, Y1467C, R1627W, A1629V
ETNK1	N244S, N244T, N244K
ETV6	Frameshift/nonsense
EZH2	Frameshift/nonsense, Q62R, N102S, F145S, F145C, F145Y, F145L, G159R, E164D, R202Q, K238E, E244K, R283Q, H292R, P488S, R497Q, R561H, T568I, K629E, Y641N, Y641H, Y641S, Y641C, Y641F, D659Y, D659G, V674M, A677G, A677V, R679C, R679H, R685C, R685H, A687V, N688I, N688K, H689Y, S690P, I708V, I708T, I708M, E720K, E740K
FLT3	V579A, V592I, F594L, FY590-591GD, D835Y, D835H, D835E, del835
GATA1	Frameshift/nonsense
GATA2	Frameshift/nonsense, R293Q, N317H, A318T, A318V, A318G, G320D, L321P, L321F, L321V, Q328P, R330Q, R361L, L359V, A372T, R384G, R384K
GATA3	Frameshift/nonsense/splice-site ZNF domain, R276W, R276Q, N286T, L348V
GNA13	I34T, G57S, S62F, M68K, Q134R, Y145F, L152F, E167D, Q169H, R264H, E273K, V322G, V362G, L371F
GNAS	R201(844)G, R201(844)S, R201(844)C, R201(844)H, R201(844)L, Q227(870)K, Q227(870)R, Q227(870)L, Q227(870)H, R374(1017)C
GNB1	K57N, K57M, K57E, K57T, I80T, I80N
IDH1	R132C, R132G, R132H, R132L, R132P, R132V
IDH2	R140W, R140Q, R140L, R140G, R172W, R172G, R172K, R172T, R172M, R172N, R172S
IKZF1	Frameshift/nonsense
IKZF2	Frameshift/nonsense
IKZF3	Frameshift/nonsense
JAK1	T478A, T478S, V623A, A634D, L653F, R724H, R724Q, R724P, T782M, L783F
JAK2	N533D, N533Y, N533S, H538R, K539E, K539L, I540T, I540V, V617F, R683S, R683G, del/ins537-539L, del/ins538-539L, del/ins540-543MK, del/ins540-544MK, del/ins541-543K, del542-543, del543-544, ins11546-547
JAK3	M511T, M511I, A572V, A572T, A573V, R657Q, V715I, V715A
KDM6A	Frameshift/nonsense/splice-site, del419
KIT	ins503, V559A, V559D, V559G, V559I, V560D, V560A, V560G, V560E, del560, E561K, del579, P627L, P627T, R634W, K642E, V654A, V654E, H697D, E761D, K807R, D816H, D816Y, D816F, D816I, D816V, D816H, del551-559
KRAS	G12D, G12A, G12E, G12V, G13D, G13C, G13Y, G13F, G13R, G13A, G13V, G13E, V14I, L19F, T58I, G60D, G60A, G60V, Q61K, Q61E, Q61P, Q61R, Q61L, Q61H, K117E, K117N, A146T, A146P, A146V
LUC7L2	Frameshift/nonsense/splice-site
MLL	Frameshift/nonsense
MLL2	Frameshift/nonsense
MPL	S505G, S505N, S505C, L510P, del513, W515A, W515R, W515K, W515S, W515L, A519T, A519V, Y591D, W515-518KT
NF1	Frameshift/nonsense
NPM1	Frameshift p.W288fs (insertion at c.859_860, 860_861, 862_863, 863_864)

NRAS	G12S, G12R, G12C, G12N, G12P, G12Y, G12D, G12A, G12V, G12E, G13S, G13R, G13C, G13N, G13P, G13Y, G13D, G13A, G13V, G13E, G60E, G60R, Q61R, Q61L, Q61K, Q61P, Q61H, Q61Q
NXF1	Frameshift/nonsense/splice-site
PDS5B	Frameshift/nonsense/splice-site, R1292Q
PHF6	Frameshift/nonsense/splice-site, A40D, M125I, S246Y, F263L, R274Q, C297Y, H302Y, H329L
PHIP	Frameshift/nonsense/splice-site
PPM1D	Frameshift/nonsense, exon 5 or 6
PRPF8	M1307I, C1594W, D1598Y, D1598N, D1598V (ADD MORE VARS)
PTEN	Frameshift/nonsense, D24G, R47G, F56V, L57W, H61R, K66N, Y68H, C71Y, F81C, Y88C, D92G, D92V, D92E, H93Y, H93D, H93Q, N94I, P95L, I101T, C105F, C105S, D107Y, L112V, H123Y, C124R, C124S, K125E, A126D, K128N, R130G, R130Q, R130L, G132D, I135V, I135K, C136R, C136F, K144Q, A151T, D153Y, D153N, Y155H, Y155C, R159K, R159S, R161K, R161I, G165R, G165E, S170N, S170I, R173C, Y174D, Y177C, H196Y, R234W, G251C, D252Y, F271S, D326G
PTPN11	G60V, G60R, G60A, D61Y, D61V, D61G, Y63C, E69K, E69G, E69D, E69Q, F71L, F71K, A72T, A72V, A72D, T73I, E76K, E76Q, E76M, E76A, E76G, E139G, E139D, N308D, N308T, N339S, P491L, S502P, S502A, S502L, G503V, G503G, G503A, G503E, Q506P, T507A, T507K
RAD21	Frameshift/nonsense/splice-site, R65Q, H208R, Q474R
RUNX1	Frameshift/nonsense/splice-site, S73F, H78Q, H78L, R80C, R80P, R80H, L85Q, P86L, P86H, S114L, D133Y, L134P, R135G, R135K, R135S, R139Q, R142S, A165V, R174Q, R177L, R177Q, A224T, D171G, D171V, D171N, R205W, R223C
SETBP1	D868N, D868T, S869N, G870S, I871T, D880N, D880Q
SETD2	Frameshift/nonsense, V1190M
SETDB1	Frameshift/nonsense, K715E
SF3B1	G347V, R387W, R387Q, E592K, E622D, Y623C, R625L, R625C, R625G, N626D, R630G, H662Q, H662D, T663I, K666N, K666Q, K666T, K666E, K666R, K700E, V701F, A708T, G740R, G740E, G742D, A744P, A745P, K748E, R775P, D781G, E783K, R831Q, L833F, E862K, R957Q
SFRS2	Y44H, P95H, P95L, P95T, P95R, P95A, P107H, P95fs
SMC1A	K190T, R586W, M689V, R807H, R1090H, R1090C
SMC3	Frameshift/nonsense, R155I, Q367E, D392V, K571R, R661P, G662C
SRCAP	Frameshift/nonsense/splice-site
STAG1	Frameshift/nonsense/splice-site, H1085Y
STAG2	Frameshift/nonsense/splice-site
SUZ12	Frameshift/nonsense
TET2	Frameshift/nonsense/splice-site, missense mutations in catalytic domains (p.1104-1481 and 1843-2002), D1121Y, D1129Y, C1133R, C1133W, C1135Y, C1135F, C1135W, G1137D, G1137V, E1137K, E1137D, E1141K, E1144K, Y1146C, L1151R, G1152R, A1153T, A1153V, G1154S, C1156Y, V1157M, I1160F, I1160S, R1161G, R1161S, M1164I, E1165K, E1165D, R1167G, R1167K, R1167S, R1167M, L1172R, A1174T, I1175T, V1180D, M1185I, E1186A, G1187S, K1188R, G1192V, C1193Y, C1193W, P1194L, P1194R, I1195V, K1197E, W1198C, W1198R, V1201I, E1207D, L1208P, L1210P, C1211Y, L1212S, V1213M, V1213E, R1214W, R1214Q, R1216Q, H1219D, H1219R, H1219Y, C1221Y, C1221R, C1221S, C1221W, C1221F, L1229R, G1235E, R1235W, L1236V, A1241S, K1243R, K1243N, L1244P, Y1245C, Y1245N, L1248P, L1248R, L1252P, L1252V, G1256C, R1261C, R1261S, R1261H, R1261P, R1262W, C1263F, C1263Y, N1266D, N1266K, N1266H, N1266Y, N1266S, C1271W, C1271S, C1273S, C1273W, C1273R, Q1274P, G1275R, G1275V, G1282R, G1282D, R1283P, S1284F, F1287V, G1288D, G1288V, C1289F, C1289W, S1290L, W1291C, S1292R, M1293I, Y1294C, G1297E, G1297R, C1298Y, C1298S, K1299M, K1299Q, K1299N, F1300V, F1300L, F1300I, S1303G, S1303R, K1310Q, L1311Q, E1318E, L1322Q, L1322P, L1322R, L1326W, L1329P, L1329Q, L1332P, M1333K, L1340R, L1340P, Y1345D, Y1345C, Q1348K, Q1348R, I1349N, E1352K, A1355V, C1358S, C1358W, R1359C, R1359L, R1359P, R1359H, R1359G, R1359S, L1360R, G1361C, G1361S, G1361D, R1366H, R1366L, R1366C, P1367L, P1367S, P1367R, F1368L, G1370V, G1370R, V1371D, A1373P, A1376V, D1376G, F1377V, F1377I, C1378R, C1378Y, C1378F, H1380Y, H1380L, H1380R, H1380Q, R1380C, H1380D, H1382R, H1382P, R1383G, H1386D, R1387H, N1387S, T1393A, C1395Y, T1397I, L1398R, F1398C, F1398L, L1398H, L1398P, H1401Y, E1401A, N1403S, Q1414R, Q1414H, Q1414K, V1416L, V1417F, P1419R, D1427V, Q1435K, V1438F, G1861E, G1861R, G1861V, A1863V, H1868Y, H1868P, H1868L, G1869W, S1870L, L1872P, I1873T, I1873S, A1876T, A1876V, R1878P, R1878H, E1879Q, E1879G, E1879D, H1881N, H1881L, T1884A, T1884I, P1889L, N1890S, P1894T, P1894R, P1894L, P1894H, R1896G, I1897N, S1898F, V1900F, E1900K, V1900D, Y1902H, Y1902C, Q1903R, A1903V, H1904R, H1904Q, K1905E, T1905A, H1912R, H1912D, H1912Y, G1913D, A1919D, F1922S, Y1923H, H1925Q, K1934N, R1966C, D1981A, S1982Y
TP53	Frameshift/nonsense/splice-site, S46F, G105C, G105R, G105D, G108S, G108C, R110L, R110C, T118A, T118R, T118I, S127F, S127Y, L130V, L130F, K132Q, K132E, K132W, K132R, K132M, K132N, F134V, F134L, F134S, C135W, C135S, C135F, C135G, C135Y, Q136K, Q136E, Q136P, Q136R, Q136L, Q136H, A138P, A138V, A138A, A138T, T140I, C141R, C141G, C141A, C141Y, C141S, C141F, C141W, V143M, V143A, V143E, L145Q, W146C, W146L, L145R, V147G, P151T, P151A, P151S, P151H, P151R, P152S, P152R, P152L, T155P, T155A, V157F, R158H, R158L, A159V, A159P, A159S, A159D, A161T, A161D, Y163N, Y163H, Y163D, Y163S, Y163C, K164E, K164M, K164N, K164P, H168Y, H168P, H168R, H168L, H168Q, M169I, M169T, M169V, E171K, E171Q, E171G, E171A, E171V, E171D, V172D, V173M, V173L, V173G, R174W, R175G, R175C, R175H, C176R, C176G, C176Y, C176F, C176S, P177R, P177L, H178D, H178P, H178Q, H179Y, H179R, H179Q, H179Q, R181C, R181Y, R181H, D186G, G187S, P190L, P190T, H193N, H193P, H193L, H193R, L194F, L194R, I195F, I195N, I195T, R196P, V197L, G199V, Y205D, Y205N, Y205C, V203M, Y205H, D208V, R213Q, R213P, F212I, R213L, R213Q, H214D, H214P, H214R, S215G, S215I, S215R, V216M, V217G, Y220N, Y220H, Y220S, Y220C, E224D, I232F, I232N, I232T, I232S, Y234N, Y234H, Y234S, Y234C, Y236N, Y236H, Y236C, M237V, M237K, M237I, C238R, C238G, C238Y, C238W, N239T, N239S, S241Y, S241C, S241F, C242G, C242Y, C242S, C242F, G244S, G244C, G244D, G245S, G245R, G245C, G245D, G245A, G245V, G245S, M246V, M246K, M246R, M246I, N247I, R248W, R248G, R248Q, R249G, R249W, R249T, R249M, P250L, I251N, L252P, I254S, I255F, I255N, I255S, L257Q, L257P, E258K, E258Q, D259Y, S261T, G262D, G262V, L265P, G266R, G266E, G266V, R267W, R267Q, R267P, E271K, V272M, V272L, R273S, R273G, R273C, R273H, R273P, R273L, V274F, V274D, V274A, V274G, V274L, C275Y, C275S, C275F, A276P, C277F, C277Y, P278T, P278A, P278S, P278H, P278R, P278L, G279E, R280G, R280K, R280T, R280I, R280S, D281N, D281H, D281Y, D281G, D281E, D281V, R282G, R282W, R282Q, R282P, E285K, E285V, E286G, E286V, E286K, K320N, L330R, G334V, R337C, R337L, A347T, L348F, T377P
U2AF1	D14G, S34F, S34Y, R35L, R156H, R156Q, Q157R, Q157P
U2AF2	R18W, Q143L, M144I, L187V, Q190L
WT1	Frameshift/nonsense/splice-site
YLPM1	Frameshift/nonsense/splice-site
ZBTB33	Frameshift/nonsense/splice-site, A9P, D11V, D11G, S15C, L19P, Q25E, Q25R, R26C, R26H, C32G, C32Y, V34G, V34D, T35P, R41Q, A45P, L50I, S54G, Y56C, Q59P, Q59K, V67I, V68D, L70R, R74G, I77F, I77N, Y86C, I90N, E100G, L108V, I113K, I113T, A114T, A114V, L116H, Y434H, Y434C, A435V, I437T, G438S, G438V, T441A, Y442C, D443G, I446S, P447A, L459F, E485D, Y494C, C496R, C496F, C496S, C496Y, R501T, Y503S, L509V, H512Y, H512R, N514K, S517C, Y522C, Y522H, R525C, Y526N, Y526D, C527R, C527Y, P532S, L533F, A534V, A534T, E535Q, E535K, E535A, R537C, R537H, R537L, T538A, T538R, H540N, E541K, H543D, H544R, E547K, R549K, Y550C, Q551P, C552G, C552Y, C555Y, Y562C, Q563P, S566P, Y584C, S591A
ZNF318	Frameshift/nonsense/splice-site
ZRSR2	Frameshift/nonsense, E133G, C181F, D185G, C187Y, H191Y, I202N, F239V, F239Y, N261Y, C280R, C302R, C326R, H330R

Table S2. TOPMed Demographics

A) Cardiovascular Health Study

	No AD (n=577)	Incident AD (n=166)
Mean Age at Blood Draw ± SD	72.8±4.95	74.3±5.01
Female	375 (65.0)	116 (69.9)
***APOE* ε2ε2 or ε2ε3**	101 (17.5)	22 (13.2)
***APOE* ε3ε3**	340 (58.9)	84 (50.6)
***APOE* ε2ε4**	17 (2.9)	9 (5.4)
***APOE* ε3ε4**	115 (19.9)	47 (28.3)
***APOE* ε4ε4**	4 (0.7)	4 (2.4)
CHIP carrier	90 (15.5)	21 (12.7)

B) Framingham Heart Study

	No AD (n=2345)	Incident AD (n=92)
Mean Age at Blood Draw ± SD	59.6±13.7	80.8±7.54
Female	1312 (55.9)	73 (79.3)
***APOE* ε2ε2 or ε2ε3**	303 (12.9)	7 (7.6)
***APOE* ε3ε3**	1532 (65.3)	52 (56.5)
***APOE* ε2ε4**	44 (1.9)	4 (4.3)
***APOE* ε3ε4**	430 (18.3)	28 (30.4)
***APOE* ε4ε4**	36 (1.5)	3 (3.3)
CHIP carrier	143 (6.1)	9 (9.8)

SD—standard deviation

Parentheses indicate percent of total of no AD or incident AD groups

Table S3. Cox proportional hazards model for risk of AD in TOPMed

A) Cardiovascular Health Study CPH model

	HR	95% CI	p-value
Age (per year)	1.12	1.08-1.15	2.8 x 10-13
***APOE* ε2ε2 or ε2ε3 (referent to APOE ε3ε3)**	0.85	0.53-1.37	0.51
***APOE* ε2ε4 (referent to *APOE* ε3ε3)**	2.11	1.04-4.24	0.037
***APOE* ε3ε4 (referent to *APOE* ε3ε3)**	2.19	1.51-3.19	3.2 x 10-5
***APOE* ε4ε4 (referent to *APOE* ε3ε3)**	1.63	0.58-4.57	0.35
Females (referent to males)	1.20	0.85-1.69	0.30
Davis site (referent to Bowman Gray)	0.87	0.46-1.64	0.67
Hopkins site (referent to Bowman Gray)	1.76	0.98-3.17	0.060
Pitt site (referent to Bowman Gray)	2.53	1.52-4.22	3.5 x 10-4
Black (referrent to white)	1.54	1.08-2.20	0.018
American Indian (referent to white)	1.43	0.20-10.4	0.72
CHIP carriers (referent to CHIP non-carriers)	0.73	0.46-1.65	0.19

B) Framingham Heart Study CPH model

	HR	95% CI	p-value
Age (per year)	1.20	1.17-1.23	<2 x 10-16
***APOE* ε2ε2 or ε2ε3 (referent to *APOE* ε3ε3)**	0.68	0.31-1.49	0.33
***APOE* ε2ε4 (referent to *APOE* ε3ε3)**	0.88	0.21-3.64	0.86
***APOE* ε3ε4 (referent to *APOE* ε3ε3)**	2.22	1.40-3.52	7.5 x 10-4
***APOE* ε4ε4 (referent to *APOE* ε3ε3)**	5.39	1.64-17.7	5.6 x 10-3
Females (referent to males)	1.66	0.98-2.81	0.062
CHIP carriers (referent to CHIP non-carriers)	0.57	0.28-1.15	0.12

C) Meta-analysis for CHIP

	HR	95% CI	p-value
CHIP carriers (referent to CHIP non-carriers)	0.69	0.47-1.02	0.060

CPH - Cox proportional hazards
HR—hazard ratio
95% CI—95 percent confidence interval

Table S4. Competing risks regression model for risk of AD in FHS including family as cluster variable

	SHR	95% CI	p-value
Age (per year)	1.19	1.16-1.22	2.8 x 10-13
***APOE* ε2ε2 or ε2ε3 (referent to APOE ε3ε3)**	0.61	0.27-1.42	0.25
***APOE* ε2ε4 (referent to *APOE* ε3ε3)**	0.97	0.20-4.64	0.97
***APOE* ε3ε4 (referent to *APOE* ε3ε3)**	2.27	0.44-1.45	3.3 x 10-4
***APOE* ε4ε4 (referent to *APOE* ε3ε3)**	5.60	1.89-16.57	1.9 x 10-3
Females (referent to males)	2.00	1.10-3.62	0.022
CHIP carriers (referrent to non-CHIP carriers)	0.51	0.24-1.05	0.068

Table S5. ADSP Demographics

A) ADSP sample

Cohort	n Controls (*APOE* ε3ε3)	n Cases (*APOE* ε3ε3)
ACT	655	215
ADC	441	516
CHAP	23	1
CUHS	95	88
LOAD	70	114
MAP	65	29
NCRD	0	42
ROS	87	49
TARC	10	50
Total	**1446**	**1104**

B) All *APOE* ε3ε3

	Controls (n=1446)	AD cases (n=1104)
Mean Age ± SD	80.5±7.07	80.3±6.89
Female	835 (57.7)	623 (56.4)
CHIP carrier (VAF>0.08)	240 (16.6)	129 (11.7)
CHIP carrier (VAF≤0.08)	60 (4.1)	60 (5.4)

SD - standard deviation
VAF - variant allele fraction

Table S6. Risk of AD in ADSP

Logistic regression model for risk of AD	OR	95% CI	p-value
Age (per year)	1.0	0.99-1.01	0.97
Females (referent to males)	0.94	0.80-1.11	0.47
CHIP (referent to CHIP non-carriers)*	0.66	0.53-0.84	5.5 x 10-4

* Those with VAF≤0.08 were considered non-CHIP)

OR - odds ratio

95% CI - 95 percent confidence interval

Table S7. Risk of AD by VAF in ADSP

A) Logistic regression model for risk of AD stratified by VAF cutoff

	OR	95% CI	p-value
Age (per year)	1.0	0.99-1.01	0.95
Females (referent to males)	0.94	0.80-1.11	0.49
CHIP VAF>0.08 (referent to CHIP non-carriers)	0.67	0.53-0.85	9.1 x 10-4
CHIP VAF≤0.08 (referent to CHIP non-carriers)	1.25	0.86-1.81	0.23

B) Linear regression model for risk of AD in CHIP carriers using VAF as a continuous variable

	OR	95% CI	p-value
Age (per year)	1.0	0.97-1.03	0.80
Females (referent to males)	0.81	0.56-1.18	0.28
log(VAF)	0.78	0.61-0.99	0.045

OR - odds ratio
95% CI - 95 percent confidence interval
VAF - variant allele fraction

Table S8. Neuropathological findings in ADSP controls without dementia or cognitive impairment

A)

CERAD neuritic plaque score	n CHIP non-c	n CHIP carriers
0	122	40
1	106	20
2	61	16
3	59	3
Total	**348**	**79**

B)

Braak stage	n CHIP non-c	n CHIP carriers
0, I, II	169	44
III, IV	135	36
V, VI	63	7
Total	**367**	**87**

C) Ordinal logistic regression model for CERAD score

	OR	95% CI	p-value
Age at autopsy (per year)	1.02	0.99-1.05	0.12
***APOE* ε2ε2 or ε2ε3 (referent to *APOE* ε3ε3)**	0.48	0.28-0.79	4.6 x 10-3
***APOE* ε2ε4, ε3ε4, or ε4ε4 (referent to *APOE* ε3ε3)**	1.50	0.93-2.40	0.093
Females (referent to males)	0.98	0.69-1.40	0.92
CHIP carriers (referent to CHIP non-carriers)	0.50	0.31-0.79	3.2 x 10-3

D) Ordinal logistic regression model for Braak stage

	OR	95% CI	p-value
Age at autopsy (per year)	1.17	1.13-1.21	6.9 x 10-18
***APOE* ε2ε2 or ε2ε3 (referent to *APOE* ε3ε3)**	1.03	0.61-1.74	0.92
***APOE* ε2ε4, ε3ε4, or ε4ε4 (referent to *APOE* ε3ε3)**	1.41	0.85-2.33	0.18
Females (referent to males)	1.03	0.71-1.51	0.86
CHIP carriers (referent to CHIP non-carriers)	0.56	0.35-0.89	0.015

OR- odds ratio

95% CI - 95 percent confidence interval

CERAD - Consortium to establish a registry for Alzheimer's disease

Table S9. Risk of AD by *APOE* genotype in TOPMed

A) CRR model for risk of AD in those with *APOE* ε2ε2 or ε2ε3

CHS	SHR	95% CI	p-value
Age (per year)	0.97	0.90-1.03	0.30
Females (referent to males)	0.69	0.30-1.57	0.38
CHIP (referent to CHIP non-carriers)	1.85	0.61-5.55	0.28
FHS	**SHR**	**95% CI**	**p-value**
Age (per year)	1.18	1.09-1.23	1.5 x 10-6
Females (referent to males)	1.85	0.16-21.5	0.62
CHIP (referent to CHIP non-carriers)	0.82	0.08-8.82	0.87

B) CRR model for risk of AD in those with *APOE* ε3ε3

CHS	SHR	95% CI	p-value
Age (per year)	1.11	1.07-1.15	2.7 x 10-9
Females (referent to males)	1.38	0.85-2.23	0.19
CHIP (referent to CHIP non-carriers)	0.55	0.27-1.10	0.09
FHS	**SHR**	**95% CI**	**p-value**
Age (per year)	1.23	1.18-1.28	<1 x 10-22
Females (referent to males)	1.66	0.82-3.36	0.16
CHIP (referent to CHIP non-carriers)	0.50	0.22-1.18	0.11

C) CRR model for risk of AD in those with *APOE* ε2ε4, ε3ε4, or ε4ε4

CHS	SHR	95% CI	p-value
Age (per year)	1.05	1.01-1.11	0.032
Females (referent to males)	1.24	0.65-2.36	0.52
CHIP (referent to CHIP non-carriers)	0.71	0.33-1.54	0.39
FHS	**SHR**	**95% CI**	**p-value**
Age (per year)	1.14	1.10-1.18	1.9 x 10-14
Females (referent to males)	2.07	0.84-5.07	0.11
CHIP (referent to CHIP non-carriers)	0.29	0.03-2.51	0.26

CRR—Competing risks regression
SHR—Subdistribution hazard ratio
95% CI—95 percent confidence interval

Table S10. Risk of AD by mutated gene

A) Logistic regression for risk of AD in TOPMed (CHS and FHS)

	OR	95% CI	p-value
Age (per year)	1.16	1.13-1.18	7.6 x 10-41
Females (referent to males)	1.70	1.24-2.34	1.0 x 10-3
FHS (referent to CHS)	0.23	0.17-0.31	2.5 x 10-22
***APOE* ε2ε2 or ε2ε3 (referent to *APOE* ε3ε3)**	0.86	0.55-1.36	0.52
***APOE* ε2ε4 (referent to *APOE* ε3ε3)**	1.62	0.76-3.46	0.21
***APOE* ε3ε4 (referent to *APOE* ε3ε3)**	2.17	1.54-3.04	7.7 x 10-6
***APOE* ε4ε4 (referent to *APOE* ε3ε3)**	4.60	1.79-11.8	1.5 x 10-3
***DNMT3A* mutation (referent to CHIP non-carriers)**	0.66	0.34-1.29	0.22
***TET2* mutation (referent to CHIP non-carriers)**	0.56	0.21-1.45	0.24
***ASXL1* mutation (referent to CHIP non-carriers)**	0.81	0.21-3.13	0.76
***SF3B1* mutation (referent to CHIP non-carriers)**	0.70	0.08-6.09	0.74
Other mutation (referent to CHIP non-carriers)	0.54	0.20-1.50	0.24
Multiple mutations (referent to CHIP non-carriers)	0.51	1.43-1.84	0.30

B) Logistic regression for risk of AD in ADSP (*APOE* ε3ε3)

	OR	95% CI	p-value
Age (per year)	1.00	0.99-1.01	0.96
Females (referent to males)	0.94	0.80-1.10	0.42
***DNMT3A* mutation (referent to CHIP non-carriers)**	0.75	0.51-1.10	0.14
***TET2* mutation (referent to CHIP non-carriers)**	0.68	0.42-1.10	0.12
***ASXL1* mutation (referent to CHIP non-carriers)**	0.55	0.25-1.22	0.14
***SF3B1* mutation (referent to CHIP non-carriers)**	0.61	0.26-1.44	0.26
Other mutation (referent to CHIP non-carriers)	0.56	0.34-0.90	0.017
Multiple mutations (referent to CHIP non-carriers)	0.73	0.39-1.37	0.33

OR- odds ratio

95% CI - 95 percent confidence interval

Table S11. Mutations detected from Whole Exome Sequencing of brain DNA in ADSP

ID	AD	*APOE*	Braak	Age	Gene	Variant Classification	Protein Change	VAF	Alt	Ref
ADSP_Brain_exome1	1	34	6	81-85	*ASXL1*	Frame Shift Insertion	p.S1166fs	0.024	5	207
ADSP_Brain_exome2	1	33	3	86-90	*BCORL1*	Nonsense Mutation	p.Y1692*	0.103	3	26
ADSP_Brain_exome3	1	33	5	86-90	*CBL*	Missense Mutation	p.C404Y	0.04	6	143
ADSP_Brain_exome4	1	33	6	86-90	*DNMT3A*	Missense Mutation	p.R366H	0.086	5	53
ADSP_Brain_exome5	1	34	5	76-80	*GATA3*	Nonsense Mutation	p.C375*	0.038	7	175
ADSP_Brain_exome6	1	34	6	66-70	*NF1*	Nonsense Mutation	p.S1786*	0.041	4	93
ADSP_Brain_exome7	1	34	6	81-85	*NXF1*	Splice Site		0.06	5	79
ADSP_Brain_exome8	0	33	1	86-90	*PRPF8*	Missense Mutation	p.C1594W	0.04	7	168
ADSP_Brain_exome9	1	34	6	81-85	*SETBP1*	Missense Mutation	p.G870S	0.032	5	150
ADSP_Brain_exome10	1	33	5	81-85	*SRSF2*	Missense Mutation	p.P95H	0.052	4	73
ADSP_Brain_exome11	1	34	5	71-75	*TET2*	Frame Shift Deletion	p.P656fs	0.081	10	114
ADSP_Brain_exome12	1	34	6	81-85	*TET2*	Nonsense Mutation	p.Q810*	0.051	7	131
ADSP_Brain_exome13	1	23	5	86-90	*TET2*	Missense Mutation	p.Q1274P	0.068	4	55
ADSP_Brain_exome14	1	23	5	86-90	*TET2*	Nonsense Mutation	p.R1465*	0.076	5	61
ADSP_Brain_exome15	1	33	6	86-90	*TET2*	Missense Mutation	p.R1366H	0.058	6	97
ADSP_Brain_exome16	0	33	0	86-90	*TP53*	Missense Mutation	p.G266R	0.089	24	247
ADSP_Brain_exome17	1	34	5	76-80	*ZBTB33*	Missense Mutation	p.Q59K	0.042	4	92

AD - Alzheimer's (0 - no, 1 - yes)
VAF - variant allele fraction
Alt - alternate allele read count
Ref - reference allele read count

Table S12. Mutations detected from sequencing of brain samples from CHIP carriers

ID	AD	Sex	Age	*APOE* genotype	Braak stage	CHIP carrier	Gene 1	Gene 2	Variant 1	Variant 2	Blood VAF 1	Blood VAF 2	Region	Unsorted Brain VAF 1	Unsorted Brain VAF 2	c-MAF+ NeuN- VAF1	c-MAF- NeuN- VAF1	c-MAF- NeuN+ VAF1	c-MAF+ NeuN+ VAF1	c-MAF+ NeuN- VAF2	c-MAF- NeuN- VAF2	c-MAF- NeuN+ VAF2	c-MAF+ NeuN+ VAF2
ACT1	1	1	86-90	33	5	yes	*DNMT3A*		p.L859*		0.07		Occipital Cortex	<0.003		<0.003	<0.003	<0.003	<0.003				
ACT2	0	1	86-90	33	3	yes	*DNMT3A*		p.R635P		0.14		Occipital Cortex	**0.0036**		**0.101**	<0.003	<0.003	<0.003				
													Cerebellum	<0.003		**0.035**		<0.003	<0.003				
ACT3	0	1	86-90	33	2	yes	*DNMT3A*		p.Y735C		0.385		Occipital Cortex	**0.02**		**0.097**	<0.003	<0.003	**0.0412**				
ACT4	0	0	81-85	33	2	yes	*SF3B1*		p.H662Q		0.18		Occipital Cortex	**0.0097**		**0.049**	**0.0073**	<0.003	**0.0061**				
													Cerebellum	**0.0039**		**0.02**	**0.0071**	<0.003	<0.003				
ACT5	0	1	86-90	33		yes	*TET2*		p.C1193Y		0.111		Occipital Cortex	**0.0069**		**0.055**	<0.003	<0.003	<0.003				
ACT6	0	0	86-90	33	2	yes	*TET2*		p.KL1818fs		0.143		Occipital Cortex	**0.011**		**0.281**	<0.003	<0.003	<0.003				
													Cerebellum	**0.0016**		**0.032**	**0.02**	<0.003	<0.003				
													Putamen	**0.017**		**0.024**	**0.015**	<0.003	**0.0043**				
ACT7	0	0	86-90	33	2	yes	*ASXL1*	*TET2*	p.S444*	p.A1355V	0.327	0.146	Occipital Cortex	**0.0076**	<0.003	**0.075**	<0.003	<0.003	<0.003	**0.025**	<0.003	<0.003	<0.003
ACT8	1	1	86-90	33	5	yes	*DNMT3A*	*GNB1*	p.T538fs	p.K57E	0.333	0.231	Occipital Cortex	<0.003	<0.003	**0.071**	<0.003	<0.003	<0.003	**0.057**	<0.003	<0.003	**0.0022**
													Putamen	<0.003	<0.003	<0.003	<0.003	<0.003	<0.003	<0.003	<0.003	<0.003	<0.003
ACT9	0	1	86-90	33	1	no							Occipital Cortex										

AD — Alzheimer's (0 - no, 1 - yes)
Sex — 0-male, 1-female
VAF — variant allele fraction

	C1	C2	C3	C4	C5	C6	C7	C8	C9	C10	C11	C12	C13	C14	C15	C16	C17	C18
ACT9 unsort OC	0	0	2423	5776	17	0	5	1	211	39	1864	3323	60	28	781	184	82	287
ACT9 sort OC	0	0	1	0	0	0	0	0	100	14	175	156	4	2	21	8	11	1
ACT6 unsort Ce	8545	850	12	0	0	0	0	0	76	0	58	26	39	22	225	72	13	49
ACT6 unsort P	2	3	233	5	6	59	559	17	97	20	15	6	344	61	255	215	56	286
ACT6 sort Ce	38	193	8	0	0	0	0	0	102	3	5	1	12	0	10	9	13	14
ACT6 sort P	0	0	2	0	0	1	1	0	17	1	0	0	34	6	51	33	9	82
ACT2 unsort OC	0	6	1092	4814	28	7	1	5	159	105	842	311	159	183	357	294	863	292
ACT2 sort OC	0	0	9	7	0	0	0	0	43	6	29	1	7	5	58	10	31	37
PD3_CTRL_SUNI	0	0	297	38	27	0	0	0	652	15	780	102	2625	1743	1022	330	111	116
PD4_CTRL_SUNI	0	0	51	1	3	0	0	1	414	83	616	135	604	879	380	138	444	152
PD9_CTRL_MDFG	0	0	1035	1168	104	0	3	2	227	18	316	101	765	1104	415	347	60	134
RCLN_CAUD_06	1	0	341	3	0	1	2622	368	783	100	400	3935	68	237	340	572	138	490
RCLN_CAUD_09	0	1	241	0	0	2	2992	124	632	14	1039	2440	110	140	323	349	101	233
RCLN_CAUD_14	0	0	159	1	4	2	1444	17	276	11	240	117	2026	2518	392	157	36	38
RCLN_HIPP_11	1	1	235	649	34	0	2	1	424	14	168	48	4195	1112	387	171	36	147
RCLN_HIPP_14	0	2	1018	113	882	15	8	6	890	17	589	400	462	2329	1556	465	283	141
RCLN_PARL	0	1	1055	2276	11	0	6	2	173	11	1210	471	252	45	63	131	18	49
RCLN_SMTG	0	3	1075	1940	5	0	6	2	250	8	1407	1141	92	34	53	188	18	51

Samples in red were generated for this study. Sample in blue are from Corces et al., *Nat Gen* 2020.

Table S14. Calculation of percentage of mutant microglia in each sample

Sample	Region	Variant	Fraction of microglia in sample	VAF	Fraction of microglia with mutations
ACT9 unsorted	Occipital cortex	None	0.013991115		
ACT9 sorted	Occipital cortex	None	0.202839757		
ACT6 unsorted	Cerebellum	TET2 p.KL1818fs	0.007609893	0.00157	0.411841845
ACT6 sorted	Cerebellum	TET2 p.KL1818fs	0.25		
ACT6 unsorted	Putamen	TET2 p.KL1818fs	0.043322912	0.0166	0.766338144
ACT6 sorted	Putamen	TET2 p.KL1818fs	0.071729958		
ACT2 unsorted	Occipital cortex	DNMT3A p.R635P	0.01670519	0.0036	0.431003774
ACT2 sorted	Occipital cortex	DNMT3A p.R635P	0.176954733		